Scaling Theory of 3-Miktoarm ABC Copolymer Micelles in Selective Solvent

E. B. Zhulina[†] and O. V. Borisov*[,†,‡]

Institute of Macromolecular Compounds, Russian Academy of Sciences, 199004 St. Petersburg, Russia, and Institut Pluridisciplinaire de Recherche sur l'Environnement et les Matériaux, UMR 5254 CNRS/UPPA, 64053 Pau, France

Received October 24, 2007; Revised Manuscript Received March 7, 2008

ABSTRACT: We present a scaling theory to describe self-assembled multicompartment structures formed by *ABC* 3-miktoarm star colopymers in a dilute solution in selective solvent. Depending on the degrees of polymerization of solvophilic (*A*) and solvophobic (*B*, *C*) arms and on the ratio between interfacial tensions at the interface between solvent and both collapsed solvophobic blocks, we delinate regions of stability of aggregates of different morphologies. In particular, we demonstrate that copolymers with longer solvophilic (*A*) block form aggregatively stable starlike micelles with phase-separated cores. Depending on the ratio of interfacial tensions at the interfaces of collapsed *B* and *C* blocks with solvent and that at the *BC* interface, the core of the starlike micelle separates either in 2 (*B*, *C*) or in 3 (*B*, *C*, *B*) domains. In the case of relatively short solvophilic blocks we predict formation of cylindrical crew-cut micelles with microphase segregated (alternating in the longitudinal direction) core.

1. Introduction

Amphiphilic block copolymers attract considerable attention due to their ability to self-assemble in selective solvent to give rise to multitude of nanostructures that are of interest for different applications.[1–3] Recently self-organized nanoaggregates of amphiphilic copolymers are amply explored in the domain of nanomedicine as potential carriers for drugs and biologically active molecules.[4] Assembly of linear *ABC* triblock terpolymer gives rise to core−shell−corona micelles with compartmentalized cores and coronas, the so-called Janus micelles and vesicles.[5] Recent advances in chemistry allowed for synthesis of amphiphilic copolymers with more complex and well-defined architecture (graft, gradient, dendritic, etc.). By combining amphiphilic properties with complex topology of the macromolecule, one can introduce quite novel features in the routes of self-assembly. Topologically complex amphiphilic macromolecules may serve as building blocks for more complex, particularly, hierarchically organized nanostructures. As an example, star-shaped terpolymers considered here may assemble into thermodynamically stable nanoaggregates which, under proper conditions, may undergo further association processes.

In this paper we focus on a star-shaped terpolymer consisting of three chemically different blocks *A*, *B*, and *C* linked together at a common junction point. Such 3-miktoarm star block copolymers were first synthesized about a decade ago[6] and investigated experimentally in melts and solutions.[7–10] However, theoretical studies of such systems are sparse.[12–15] The theoretical papers on 3-miktoarm star block copolymers focused mostly on the analysis of possible microphases in a melt and respective ranges of their stability. A variety of different morphologies were predicted (lamella, polygonal cylinders, perforated layer, lamella-in-sphere, etc.). Computer simulation of such systems[15] demonstrated that in all phases junction point monomers of *ABC* miktoarm star copolymers gather on lines where three interfaces (*A*/*B*, *A*/*C*, and *B*/*C*) meet. Recent Monte Carlo modeling of *ABC* 3-miktoarm star copolymers in the solution[16] revealed the appearance of the spherical, cylindrical, and pearl-necklace micelles at relatively low volume fractions of polymer. The structure of these aggregates was sensitive to the degrees of polymerization of the blocks, the values of interaction parameters, and volume fraction of polymer. Tercopolymer with relatively long soluble block *A* gave rise to mostly spherical aggregates. A decrease in the length of the solvophilic block *A* led to formation of pearl-necklace wormlike aggregates with alternating *B* and *C* compartments and spatial networks of micelles. However, the details of micelle organization (aggregation number, periodicity of the compartments in wormlike structures, etc.) were not specified.

In this paper we develop an analytical scaling theory to describe self-assembly of *ABC* 3-miktoarm tercopolymer into micelles in a dilute solution. We focus on the case when blocks *B* and *C* are poorly soluble in a solvent (*S*) which is a good solvent for the block *A*, and all the three components *A*, *B*, and *C* are strongly incompatible. As we demonstrate below, depending on the molecular weight of soluble block *A* and strength of *B*−*S*, *C*−*S*, and *B*−*C* interactions, such copolymers associate in a dilute solution in thermodynamically stable spherical or cylindrical multicompartment micelles with microphase segregated core. We derive the power law dependences for equilibrium structural parameters of such micelles and construct a phase diagram of the system to delineate the conditions of their thermodynamic stability.

2. Model

We consider aggregates (micelles) self-assembled in dilute solution of *ABC* 3-miktoarm star copolymer. The degrees of polymerization of the blocks (star arms) *A*, *B*, and *C* are $N_A, N_B, N_C \gg 1$, respectively. In this paper we focus on the situation when the solvent is good for *A* arms and is poor for arms *B* and *C*. We assume for simplicity that both of the condensed components *B* and *C* contain the same polymer volume fraction $\varphi \simeq 1$. We assume also that components *A*, *B*, and *C* are equally incompatible (Flory−Huggins interaction parameters $\chi_{BC} = \chi_{AC} = \chi_{AB} = \chi$) and consider a symmetric case when $N_B = N_C$ whereas N_A can be arbitrary.

Because of poor solubility of the *B* and *C* arms, the 3-miktoarm stars assemble in the solution, giving rise to aggregates (micelles) consisting of condensed and mutually

* Corresponding author. E-mail: borisov@univ-pau.fr.
† Russian Academy of Sciences.
‡ UMR 5254 CNRS/UPPA.

10.1021/ma702369g CCC: $40.75
Published on Web 07/03/2008

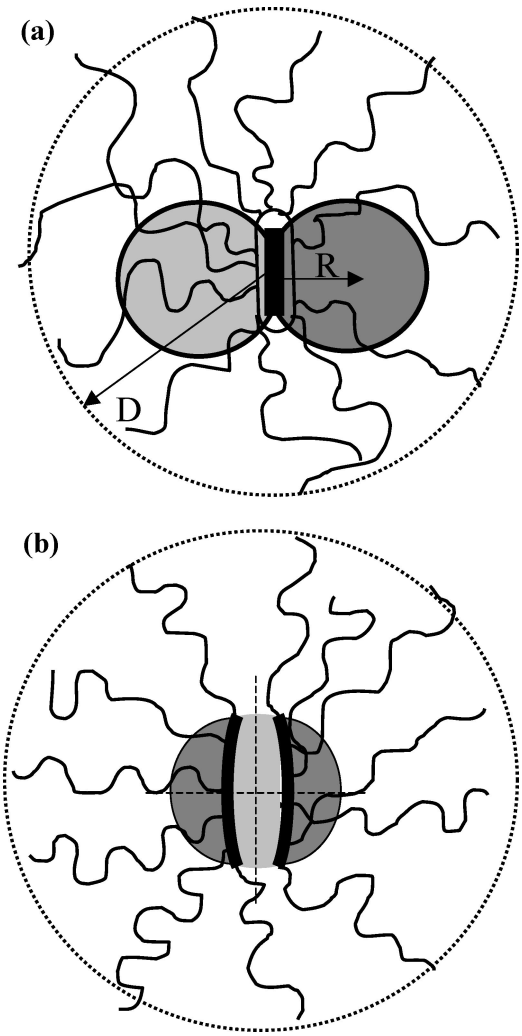

Figure 1. Schematics of a dumbbell-like micelle formed by 3-miktoarm star copolymers: (a) symmetric case of equal solvophobicity of the core-forming blocks B and C, $\alpha_C = \alpha_B$, and (b) asymmetrical case when block C forming central core domain is more solvophobic then block B, $\alpha_C > \alpha_B$.

segregated domains B and C decorated by swollen coronas formed by arms A. Spatial segregation of the A, B, and C components leads to formation of B/C, $A(S)/C$, and $A(S)/B$ boundaries.

Interfacial width of the B/C boundary is $\Delta_{BC} \simeq a\chi^{-1/2}$ whereas the surface free energy per unit area is $\gamma_{BC} \equiv \gamma \simeq k_B T a^{-2}\chi^{1/2}$ when $\chi < 1$ (the monomer size a is assumed to be the same for all the three components). At $A(S)/C$ and $A(S)/B$ boundaries polymers B and C contact mostly with the solvent, S, because volume fraction of polymer A at these boundaries is small $\varphi_A \ll 1$. These boundaries are characterized by the surface free energies per unit area $\gamma_{CS} \equiv \gamma_C$ and $\gamma_{BS} \equiv \gamma_B$, respectively. At this stage we introduce reduced surface tensions $\alpha_i = \gamma_i/\gamma$ ($i = B, C$) that characterize relative incompatibilities of the core-forming blocks B and C.

Below we focus mostly on the case of equal solvophobicities of blocks B and C, $\alpha_B \approx \alpha_C \equiv \alpha$. The case with different solvophobicities of the core-forming blocks, $\alpha_C \gg \alpha_B$, is considered in Appendix A and will be discussed separately at the end of the paper. Typical structures of micelles formed in these two cases are schematically presented in parts a and b of Figure 1, respectively. The incompatibility between two core-forming blocks B and C is typically weaker than their incompatibility with solvent S, and therefore, we mostly focus on the case of $\alpha \gtrsim 1$ values throughout the paper. However, in

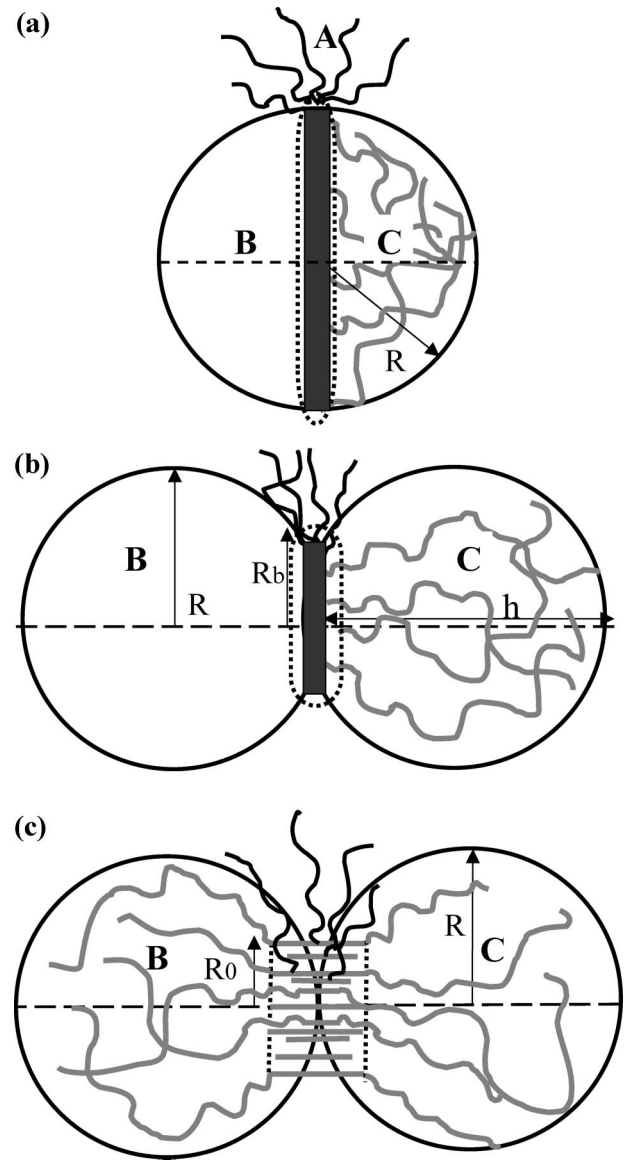

Figure 2. Schematics of a dumbbell-like micelle with equally solvophobic core-forming blocks ($\alpha_C = \alpha_B = \alpha$) in cases of weak, $\alpha \gg 1$ (a), and strong, $\alpha \leq 1$ (b, c), incompatibilities between core-forming blocks B and C.

Appendix B we also consider the case of strong incompatibility between core-forming blocks, $\alpha \ll 1$.

In contrast to diblock copolymer micelle where junctions between soluble and insoluble blocks are uniformly distributed in the interfacial layer enveloping the surface of the core, junctions in the micelles formed by 3-miktoarm star macromolecules are concentrated in a narrow beltlike layer encircling B/C boundary (Figure 2a). Such gathering of junctions allows for spatial separation of components B and C within micellar core and reduction of unfavorable $B-C$ contacts. The organization of a micellar core with beltlike and uniform distributions of junctions and the corresponding free energies of $B-C$ interactions are discussed in Appendix C. Because of incompatibility of all the components, the junction layer comprises only short segments of all the blocks, and high solubility of component A pushes the junctions closer to the external boundary of this region. We assume for simplicity that the junction monomers are localized at the external (facing solvent) boundary of the beltlike layer (within distance $\simeq a$). Investigation of specific shape of the interfacial layer is beyond the scope of this paper. In the framework of scaling type modeling we

approximate it by a torus-shaped circular ribbon with a cross section of width l and radius R_b (shown by dotted line in Figure 2a) and assume dense packing of junction points at its surface, $\pi l R_b/p \simeq a^2$, where p is the number of miktoarm stars in a micelle (aggregation number).

The free energy per macromolecule in a micelle F yields

$$F = F_{\text{surface}} + F_{\text{junc}} + F_{\text{corona}} + F_{\text{core}} \quad (1)$$

where F_{surface} is the surface free energy of the core, F_{junc} is the free energy penalty associated with the belt of junctions, F_{corona} is the free energy of coronal block A, and F_{core} is the free energy of the core blocks B and C.

3. Micelles with Dumbbell Core

Depending on the ratio of molecular weights N_A/N_B, N_C and relative surface tension on the B/S, C/S, and B/C interfaces, the 3-miktoarm star copolymer molecules can self-assemble to form micelles with cores of different shapes.

In a symmetric case $\alpha_B \approx \alpha_C \equiv \alpha$ spatial segregation of condensed blocks B and C gives rise to a symmetric dumbbell-shaped core of the micelle with radius $R \gg \Delta_{BC}$ and radius of B/C boundary $R_b \leq R$ (Figure 1a).

3.1. Free Energy. *3.1.1. Interfacial Free Energy.* By approximating the symmetric dumbbell-like core by two spherical segments of radius R and height h (see Figure 2b), we find that area of the B/C boundary is given by $\pi R_b^2 = \pi(2hR - h^2)$, whereas the total surface area of the core exposed to the solvent yields $4\pi Rh$.

In the symmetric case, $\gamma_B = \gamma_C$, the interfacial contribution to the free energy can be presented as

$$\frac{F_{\text{surface}}}{k_B T} = \frac{\gamma\pi(2hR - h^2) + \gamma_{B,C} 4\pi Rh}{pa^2} \quad (2)$$

The aggregation number p (number of macromolecules in a micelle) is given by

$$p = \frac{V\varphi}{2N_C a^3} = \frac{\pi h(hR - h^2/3)}{N_C a^3} \quad (3)$$

where $V = V_C + V_B = 2\pi h(hR - h^2/3)$ is total volume of the core. It is convenient to characterize the core shape by dimensionless ratio

$$z = \frac{h}{R} \quad (4)$$

which varies from $z = 1$ for perfectly spherical core consisting of a hemisphere B and a hemisphere C to $z = 2$ for a dumbbell-like core consisting of two spheres (B and C). Then using eq 3, we can express R and R_b as functions of p and z

$$R = a\left(\frac{pN_C}{\pi}\right)^{1/3} \frac{1}{(z^2 - z^3/3)^{1/3}} \quad (5)$$

$$R_b = R\sqrt{z(2-z)} \quad (6)$$

By substituting R from eq 5 in the surface free energy, eq 2, we find

$$\frac{F_{\text{surface}}}{k_B T} = \gamma\pi^{1/3} \frac{N_C^{2/3}}{p^{1/3}} \frac{z(2+4\alpha) - z^2}{(z^2 - z^3/3)^{2/3}} = \gamma \frac{N_C^{2/3}}{p^{1/3}} g(z, \alpha) = \frac{\gamma_{B,C}}{\alpha} \frac{N_C^{2/3}}{p^{1/3}} g(z, \alpha) \quad (7)$$

where

$$g(z, \alpha) = \left[\pi \frac{(2 + 4\alpha - z)^3}{z(1 - z/3)^2}\right]^{1/3} \quad (8)$$

and $\alpha = \gamma_{B,C}/\gamma$ is the ratio of surface tensions at the external surface of the core and at the internal B/C boundary.

As we demonstrate below, when $\alpha \gg 1$, the spherical core of micelle comprises two hemispheres, B and C, and $R_b = R = h$. This shape of the core enables to minimize the area of the B/S and C/S interfaces whereas the excess free energy of the B/C interface is negligible. In the opposite limit of strong incompatibility of the B and C blocks, $\alpha \leq 1$, the B and C blocks are well separated and form a dumbbell core consisting of nearly spherical subcores B and C. Here, $R_b \ll R$.

3.1.2. Junction Free Energy. When $\alpha \gtrsim 1$, the junction belt is envisioned as a ribbon with cross section of thickness l and inner radius $R_b = R[z(2 - z)]^{1/2}$. The volume of this ribbon, $V_{\text{junc}} \simeq l^2 R_b$, is densely packed with segments comprising $\delta n_B \approx \delta n_C \approx \delta n$ monomers of B and C blocks ($V_{\text{junc}} \simeq pa^3\delta n$). With the accuracy of numerical prefactor the surface area of the junction belt is $lR_b \simeq a^2 p$. We therefore find $\delta n \simeq l/a$, and the segments of B and C blocks comprising the belt are strongly stretched (the free energy of the elastic stretching per B (or C) segment is $F_{\text{junc,el}}/k_B T \simeq l^2/a^2\delta n \simeq l/a \gg 1$). Interaction free energy per segment $F_{\text{junc,int}}/k_B T \simeq \delta n\chi \simeq l\chi/a$ and the total free energy penalty $F_{\text{junc}} = F_{\text{junc,int}} + F_{\text{junc,el}}$ per macromolecule yields

$$\frac{F_{\text{junc}}}{k_B T} \simeq l(1 + \chi)/a \simeq \frac{a(1 + \chi)p}{R_b} \quad (9)$$

where the numerical coefficients on the order of unity are omitted. Expression 9 is applicable when $F_{\text{junc}} \ll F_{\text{surface}}$.

3.1.3. Corona Free Energy. To specify the free energy of the coronal block A, we use the scaling blob model of spherical and cylindrical brushes. In the framework of this model the corona is represented as a system of densely packed blobs with r-dependent size $\xi(r)$ and density of the free energy $k_B T/\xi^3(r)$. Free energy F_{corona} in the units of $k_B T$ is calculated as total number of blobs in the corona.

Starlike Corona. When corona thickness $H = D - R$ is much larger than the core of the micelle $\sim R$, i.e., $H \gg R$, the micelle is starlike. The corona of such micelle is envisioned as an array of concentric shells of blobs with the size $\xi(r) \simeq r^{1/2}/p^{1/2}$ growing in the radial direction.[17,18] Thickness of a starlike corona is given by

$$H_A \simeq aN_A^{3/5} p^{1/5} \quad (10)$$

whereas the free energy per molecule yields

$$\frac{F_{\text{corona}}}{k_B T} \simeq p^{1/2} \ln\left(\frac{H_A}{R}\right) \quad (11)$$

Note that in scaling terms localization of junction points in the belt encircling B/C boundary as well as deviation of the shape of the core from the spherical one does not affect the dominant power law dependence in the coronal free energy, $F_{\text{corona}} \simeq p^{1/2}$.

Crew-Cut Corona. In the opposite limit $H \ll R$ of relatively short corona-forming blocks the corona is of a crew-cut shape. Here, the distribution of the junction points on the core−corona interface determines the free energy of coronal block A.

In the case of $\alpha > 1$ and $R_b \approx R$, the corona is envisioned as a semicylindrical "bottle"-brush formed by blocks A and encircling the equator of the spherical core of radius R.

The linear grafting density (equal to the number of junction points per unit length in the semicylindrical brush) is $\rho = p/2\pi R_b \simeq l/a^2$. Because $H \ll R_b \approx R$, the structure of such a brush is virtually unaffected by curvature of the core. (The corona constitutes half of a cylindrical brush with linear grafting density $\rho \simeq l/a^2$.) The free energy of such a brush is given by[19]

$$\frac{F_{\text{corona}}}{k_{\text{B}}T} \simeq N_A^{3/8}(l/a)^{5/8} = N_A^{3/8}(ap/R_b)^{5/8} \tag{12}$$

whereas its thickness is

$$H_A \simeq N_A^{3/4}(l/a)^{1/4} = N_A^{3/4}(ap/R_b)^{1/4} \tag{13}$$

Note that when $\alpha < 1$ and $R_b \ll R$, the entire coronal blocks (in the case of crew-cut micelles) or their segments proximal to the junction points (in the case of starlike micelles) are additionally confined in a slit between the two spherical segments forming a dumbbell-shaped core. This case is considered separately in Appendix B.

3.1.4. Core Free Energy. The free energy of the core blocks *B* and *C* comprises the contribution due to the attractive monomer−monomer interactions ($\sim N_C$) and that due to the elastic stretching of the *B* and *C* chains in the core of a micelle. Because the free energy of attractive interactions does not depend on aggregation number *p*, we omit this contribution from further consideration.

When junctions are localized in the ribbon with radius $R_b \approx R$, the penalty $F_{\text{core, el}}$ due to strong local elastic stretching of the core blocks in the vicinity of the interface can be larger than the elastic free energy of a Gaussian chain with end-to-end distance $\simeq R$. Similarly to the corona-forming *A* blocks, at distances $r \ll R$ away from the junctions belt, segments of the core-forming blocks *B* and *C* can be envisioned as tethered to a ribbon on a planar surface with linear grafting density $\rho \simeq p/R_b$. Because of dense packing of the *B* and *C* monomers in the core, $\varphi = 1$, local stretching of a chain d*r*/d*n* at distance *r* from the junctions belt (axis of the semicylindrical brush) is

$$\frac{\mathrm{d}r}{\mathrm{d}n} \simeq \frac{\rho a^3}{r} \qquad l \ll r \ll R \tag{14}$$

Therefore, the free energy of local elastic stretching $F_{\text{core,el}}$ can be estimated as[20]

$$\frac{F_{\text{core,el}}}{k_{\text{B}}T} \simeq \frac{3}{2a^2}\int_l^{R_b} \frac{\mathrm{d}r}{\mathrm{d}n}\,\mathrm{d}r \simeq \frac{pa}{R_b}\ln\left(\frac{R_b}{l}\right) \simeq \frac{R^2}{a^2N_C}\ln\left(\frac{R^2}{a^2p}\right) \tag{15}$$

and the last equality assumes $R_b \simeq R$, which is valid at $\alpha \geq 1$. Therefore, when $\alpha \geq 1$, the core free energy F_{core} can be evaluated as

$$\frac{F_{\text{core}}}{k_{\text{B}}T} \simeq \frac{F_{\text{core,el}}}{k_{\text{B}}T} \simeq \frac{R^2}{a^2N_C}\ln\left(\frac{R^2}{a^2p}\right) \tag{16}$$

Note that eq 16 serves as an approximate estimate for the core free energy. It does not account for perturbation of the external parts of the core blocks due to geometric constraint on overall spherical shape of the core. However, this contribution should be on the order of the elastic free energy of a core block inside the sphere of radius *R* ($\simeq R^2/a^2N_C$). With the accuracy of the logarithmic correction in eq 16, the total free energy of a core block is, therefore, $F_{\text{core}}/k_{\text{B}}T \simeq R^2/a^2N_C$. Below we use this estimate for F_{core} to demonstrate that in a starlike micelle the core contribution can be neglected with respect to the corona and the surface free energies.

3.2. Starlike Micelle with a Dumbbell Core. We assume (and later prove) that, similarly to the case of starlike micelles formed by *AC* (or *AB*) diblock copolymers, the elastic contribution due to the core-forming blocks in a starlike micelle of *ABC* 3-miktoarm tercopolymer can be neglected. The relevant contributions to the free energy of a starlike micelle per macromolecule are

$$F \simeq F_{\text{surface}} + F_{\text{junc}} + F_{\text{corona}} \tag{17}$$

Depending on the incompatibility of the core-forming blocks, i.e., on the value of α, two different cases should be distinguished here:

3.2.1. Weak Incompatibility between B and C Blocks, $\alpha \gtrsim 1$. In this case $F_{\text{junc}} \ll F_{\text{surface}}$ and by minimizing the free energy per chain $F \approx F_{\text{surface}} + F_{\text{corona}}$ (eqs 17, 7, and 11) with respect to *p* and *z*, we determine the equilibrium aggregation number and the parameters characterizing the core shape in a starlike micelle

$$z_{\text{eq}} = \frac{2\alpha+1}{2\alpha} \to \begin{cases} 2, & \alpha \to 1/2 \\ 1, & \alpha \gg 1 \end{cases} \tag{18}$$

$$g(z_{\text{eq}}, \alpha) \simeq (9\pi)^{1/3}(1+2\alpha)^{2/3}(4\alpha-1)^{1/3} \to \begin{cases} (36\pi)^{1/3}, & \alpha \to 1/2 \\ (72\pi)^{1/3}\alpha, & \alpha \gg 1 \end{cases} \tag{19}$$

$$R_b = R\sqrt{z_{\text{eq}}(2-z_{\text{eq}})} = R\,\frac{\sqrt{4\alpha^2-1}}{2\alpha} \to \begin{cases} 0, & \alpha \to 1/2 \\ R, & \alpha \gg 1 \end{cases}$$

$$p_{\text{eq}} \sim \left(\frac{\gamma}{K}\right)^{6/5} N_C^{4/5} g(z_{\text{eq}}, \alpha)^{6/5} \simeq \left(\frac{\gamma_{\text{B,C}}}{K}\right)^{6/5} N_C^{4/5}, \quad \alpha \gg 1 \tag{20}$$

where $K \equiv \ln(H_A/R) > 1$.

As expected, in the case of weak incompatibility ($\alpha \gg 1$) between core-forming blocks *B* and *C*, the core has almost spherical shape ($z \to 1$, $R_b \to R$) (Figure 2a). On the contrary, the boundary between condensed domains *B* and *C* vanishes upon an increase in incompatibility of the core-forming blocks (when $\alpha \to 1/2$, $z \to 2$, and $R_b \to 0$) (Figure 2b).

The corresponding free energy yields

$$\frac{F_{\text{star}}}{k_{\text{B}}T} \simeq K^{2/5}\gamma^{3/5}N_C^{2/5}g(z_{\text{eq}}, \alpha)^{3/5} \simeq K^{2/5}\gamma_{B,C}^{3/5}N_C^{2/5} \tag{21}$$

whereas equilibrium core radius *R* and corona thickness *H* are given by

$$R_{\text{eq}}/a \simeq \left(\frac{\gamma}{K}\right)^{2/5} N_C^{3/5} g(z_{\text{eq}}, \alpha)^{2/5} \simeq \left(\frac{\gamma_{\text{B,C}}}{K}\right)^{2/5} N_C^{3/5} \tag{22}$$

$$H_{\text{eq}}/a \simeq \left(\frac{\gamma}{K}\right)^{6/25} N_C^{4/25} N_A^{3/5} g(z_{\text{eq}}, \alpha)^{6/25} \simeq \left(\frac{\gamma_{\text{B,C}}}{K}\right)^{6/25} N_C^{4/25} N_A^{3/5} \tag{23}$$

We therefore find familiar asymptotic power law dependences obtained previously for *AC* starlike micelle.[19]

When α is below unity ($1/2 < \alpha < 1$), radius R_b of the junction belt rapidly decreases upon a decrease in α (an increase in χ), and as a result, F_{junc} increases as

$$\frac{F_{\text{junc}}}{k_{\text{B}}T} \simeq \frac{ap\chi}{R_b} \simeq \frac{ap\chi}{R\sqrt{\alpha}} \simeq \frac{ap\chi^{5/4}}{R\gamma_{\text{B,C}}^{1/2}} \simeq N_C^{1/5}\gamma_{\text{B,C}}^{3/10}\chi^{5/4} \tag{24}$$

because of stronger stretching of the *B* and *C* chain segments proximal to the junction points. The junction belt free energy F_{junc} would become larger than $F_{\text{surface}} \simeq F_{\text{corona}} \simeq \gamma_{B,C}^{3/5}N_C^{2/5}$ when

$$\chi \geq \chi' \simeq N_C^{4/25}\gamma_{\text{B,C}}^{6/25} \tag{25}$$

Note that for $N_C \simeq 10^3$ and $\gamma_{B,C} \simeq 1$, $\chi' \simeq 3$ (recall that the numerical coefficients are omitted), and χ' is not dramatically high. In order to decrease the corresponding free energy penalty at high values of χ junctions detach from the core surface by pulling strings of *B* and *C* monomers from the cores of the micelle. The specific details of this transition are beyond the scope of this paper. However, we demonstrate in Appendix B

that even in the limit $\chi \gg 1$ the scaling exponents in eqs 20−23 are retained. Here, we review this case only briefly.

3.2.2. Strong Incompatibility between B and C Blocks, $\alpha < 1$. When α becomes smaller than one, the area of the interface between *B* and *C* collapsed blocks rapidly decreases, and finally (at $\alpha \leq 1/2$) the micellar core splits into two separate spherical subcores of *B* and *C* ($z = 2$, $R_b = 0$). Such core configuration can be attained when junctions are pulled out from the interface (Figure 2c). Each junction is now attached by strings (strongly stretched segments) of monomers *B* and *C* to the corresponding subcores. The strings form junction belt with radius $R_0 \ll R$.

Confinement of soluble blocks *A* between the subcores of *B* and *C* leads to the increase in the coronal free energy. To relax this confinement, the subcores can adjust their shapes. Determination of the exact shape of the core corresponding to the minimum in the free energy per macromolecule in the micelle is a complicated problem. We use the following approximation to describe configuration of the micellar core when $\alpha \simeq 1/2$. Each subcore is envisioned as a deformed sphere of radius *R* (see Figure 6). Inside the junction belt of radius R_0 the subcore is spherical. Outside of the junction belt the subcore is modeled as a truncated cone with height h_{cone} and radii of the bases R_0 and *R*. The cone is finally crowned by half-sphere of radius *R*. Although such shape of the core is not necessarily optimal, we demonstrate that in the framework of this approximation the scaling asymptotes for a starlike micelle with $\alpha \gg 1$ remain valid also when $\alpha < 1$.

The free energy $F = F_{corona} + F_{surface} + F_{belt} + F_{core}$ per chain in such a micelle is calculated in Appendix B

$$\frac{F_{core}}{k_BT} \simeq \frac{R^2}{a^2 N_C} x^{-1} \tag{26}$$

$$\frac{F_{surface}}{k_BT} \simeq \frac{\gamma_{B,C} N_C^{2/3}}{p^{1/3}}[1 - 0(x)] \tag{27}$$

$$\frac{F_{corona}}{k_BT} \simeq p^{1/2}\left[\ln\left(\frac{H_A}{R}\right) + \ln\left(\frac{1}{x}\right)\right] \tag{28}$$

$$\frac{F_{belt}}{k_BT} \simeq p^{1/2} + x^2 (pN_C)^{1/3} \tag{29}$$

where $x = R_0/R \ll 1$ and $0(x)$ is variable on the order of *x*. By minimizing the free energy $F \approx F_{corona} + F_{surface} + F_{belt}$ with respect to *x* and *p*, we find the radius of the junction belt

$$R_0 \simeq \sqrt{\gamma_{B,C} N_C} \tag{30}$$

and scaling asymptotes (eqs 20−23) for equilibrium parameters of a starlike micelle with $\alpha \ll 1$.

By estimating the elastic contribution of the core blocks, eqs 16 and 26, we find that asymptotically ($N_A, N_C \to \infty$) F_{core} remains smaller than $F_{surface} \simeq F_{corona}$ at any value of $\alpha < 1$ or $\alpha > 1$. However, for finite values of N_C and $\alpha < 1$ core contribution F_{core} can be numerically comparable to $F_{surface} \simeq F_{corona}$, and a more accurate calculation of the free energy would be necessary.

Starlike micelles are stable against aggregation in a dilute solution due to repulsion between extended spherical coronas, $H \gg R$. A starlike micelle transforms into a crew-cut micelle when $H \simeq R$ or

$$N_A \leq N_A^* \simeq \gamma_{B,C}^{4/15} N_C^{11/15} \tag{31}$$

3.3. Crew-Cut Micelle with a Dumbbell Core. For a crew-cut micelle with corona thickness $H \ll R$ localization of the junction points in the belt encircling *B*/*C* boundary becomes crucial. When $\alpha \gtrsim 1$, the coronal and the surface free energies per macromolecule in such a micelle are given by eqs 12 and 7, whereas aggregation number *p* is related to core radius *R* by

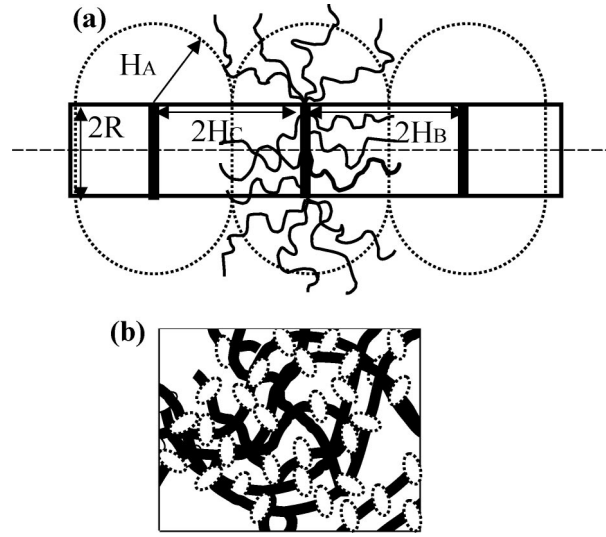

Figure 3. Schematics of cylindrical crew-cut micelle with longitudinally microphase separated *B*/*C* core (a) and precipitated phase consisting of cylindrical aggregates, $N_A < N_A^*$, $1 < \alpha < \alpha^*$ (b).

eq 5. Minimization of the total free energy with omitted logarithmic *z* dependence

$$\frac{F}{k_BT} \approx \frac{F_{surface}}{k_BT} + \frac{F_{corona}}{k_BT} \simeq \gamma_{B,C}\frac{N_C^{2/3}}{p^{1/3}} + N_A^{3/8}\left(\frac{p^{2/3}}{N_C^{1/3}}\right)^{5/8} \tag{32}$$

with respect to *p* leads to

$$p \simeq \gamma_{B,C}^{4/3}\frac{N_C^{7/6}}{N_A^{1/2}} \tag{33}$$

$$R \simeq a\gamma_{B,C}^{4/9}\frac{N_C^{13/18}}{N_A^{1/6}} \tag{34}$$

and

$$\frac{F}{k_BT} \simeq \gamma_{B,C}^{5/9} N_C^{5/18} N_A^{1/6} \tag{35}$$

The core of such a micelle is not protected by the corona because

$$H_A \simeq aN_A^{3/4}(pa/R)^{1/4} \simeq a\gamma_{B,C}^{2/9} N_C^{1/9} N_A^{2/3} \leq R$$

when $N_A \ll N_A^*$. Therefore, merge of two similar (*B*−*B* or *C*−*C*) semicores of different micelles does not cause an increase in coronal free energy F_{corona} but leads to substantial decrease in surface free energy $F_{surface}$. Simple merge of the cores and formation of aggregates comprising "sticked together" crew-cut spherical micelles leads to a decrease in the free energy per chain $\Delta F \simeq F$. A stronger decrease in the free energy is achieved when crew-cut micelles rearrange and give rise to a cylindrical micelle. Below we consider equilibrium parameters of such an aggregate and analyze conditions of its thermodynamic stability.

4. Cylindrical Micelle

To specify the scaling dependences for parameters of a cylindrical micelle, we assume that when $\alpha \geq 1$ the core constitutes a laterally segregated cylinder of radius *R* and periodicity $2H_C = 2H_B$ (Figure 3a). The radius of the *B*/*C* boundary $R_b \approx R$. Half-period H_C is related to radius *R*, aggregation number (per period) *p*, and degree of polymerization $N_B = N_C$ of the core-forming blocks as

$$H_C = \frac{a^3 p N_C}{\pi R^2} \tag{36}$$

Surface free energy per molecule in a such a cylinder yields

$$\frac{F_{\text{surface}}}{k_B T} = \gamma \frac{\pi R^2}{a^2 p} + \gamma_{B,C} \frac{4\pi R H_C}{a^2 p} = \gamma \frac{\pi R^2}{a^2 p} + \gamma_{B,C} \frac{4 N_C a}{R} \tag{37}$$

whereas the corona is envisioned as a swollen planar brush of blocks *A*

$$\frac{F_{\text{corona}}}{k_B T} \simeq N_A (s/a^2)^{-5/6} \simeq N_A \left(\frac{R}{a N_C}\right)^{5/6} \tag{38}$$

Here

$$s = \frac{2\pi R H_C}{p} = \frac{2 N_C a^3}{R} \tag{39}$$

is the "grafting" area per block *A* at the surface of the cylindrical core.

The total free energy per macromolecule yields

$$\frac{F}{k_B T} = \gamma \frac{\pi R^2}{a^2 p} + \gamma_{B,C} \frac{4 N_C a}{R} + N_A \left(\frac{R}{a N_C}\right)^{5/6} \tag{40}$$

As follows from eq 40, free energy $F(R, p)$ is a monotonically decreasing function of p. Therefore, aggregation number p (per period) should be kept at its maximal value that still ensures the applicability of eq 40 (that is, $H_A \gtrsim H_C$). By neglecting the first term in eq 40 and balancing the second and the third terms with respect to R, we find

$$R_{\text{cyl}} \simeq a \gamma_{B,C}^{6/11} \frac{N_C}{N_A^{6/11}} \tag{41}$$

$$H_{\text{cyl,C}} \simeq H_{\text{cyl.A}} \simeq a \gamma_{B,C}^{2/11} N_A^{9/11} \tag{42}$$

$$p_{\text{cyl}} \simeq \gamma_{B,C}^{14/11} \frac{N_C}{N_A^{3/11}} \tag{43}$$

and the corresponding equilibrium free energy per chain

$$\frac{F_{\text{cyl}}}{k_B T} \simeq N_A^{6/11} \gamma_{B,C}^{5/11} \tag{44}$$

Equations 41−44 indicate that the scaling dependences for all the equilibrium parameters of a cylindrical micelle coincide with those for crew-cut aggregates (sphere, cylinder, lamella) formed by diblock copolymer *AC*.[19]

Because the coronas are kept at the overlap threshold ($H_A \gtrsim H_C$) and shield the core, such micelles are expected to be stable against aggregation and remain in the form of wormlike cylinders in a dilute solution (Figure 3a). Comparison of eqs 34 and 35 with corresponding eqs 41−44 indicates the smaller value of the free energy, the larger radius of the core R and smaller aggregation number p (per period) in the cylindrical micelle than in a spherical one. In contrast to a spherical micelle where p and R are interrelated as $R \simeq a(pN_C)^{1/3}$, local cylindrical symmetry of a wormlike aggregate allows for simultaneous increase in R and decrease in p due to variation (decrease) in periodicity $H_C < R$.

By substituting p_{eq} and R_{eq} in eq 40, we find that the first term in eq 40 (the surface free energy due to *B*/*C* boundary) is negligible with respect to two other terms when $N_A/N_A^* \gg \alpha^{-11/15}$. The condition

$$N_A/N_A^* \simeq \alpha^{-11/15} \tag{45}$$

determines the lower boundary for the regime of stability of the cylindrical micelles.

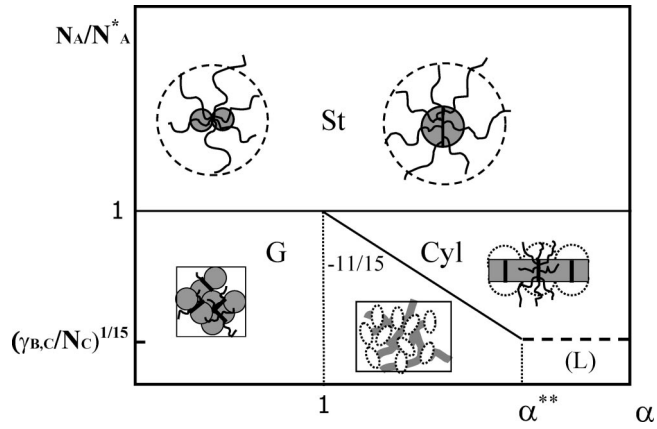

Figure 4. Diagram of states of the solution of 3-miktoarm *ABC* tercopolymer for the case of equal solvophobicities of core-forming blocks *B* and *C*. Different regions in the diagram correspond to thermodynamically stable starlike micelles with dumbbell-shaped core (region *St*), cylindrical micelles with longitudinally microphase separated core (region *Cyl*), and sediment (region *G*).

When $N_A/N_A^* \ll \alpha^{-11/15}$, an increase in the surface free energy contribution due to *B*/*C* boundary leads to a decrease in the core radius R and split of planar-like corona *A* into separate "semi-bottle-brush" coronas encircling the cylindrical *BC* core. It is instructive to obtain the scaling dependences for the parameters of such an aggregate. The free energy per chain in such a micelle yields

$$\frac{F}{k_B T} = \gamma \frac{\pi R^2}{a^2 p} + \gamma_{B,C} \frac{4 N_C a}{R} + \frac{N_A^{3/8} p^{5/8}}{(R/a)^{5/8}} \tag{46}$$

where the first and the second terms are the same as in eq 40 whereas the third term is free energy F_{corona} of a cylindrical corona, eq 12. Minimization of total free energy $F = F(p, R)$ with respect to two independent variables p and R provides the equilibrium parameters of the micelle

$$p \simeq \gamma_{B,C}^{4/3} \frac{N_C^{7/6}}{\alpha^{1/6} N_A^{1/2}} \tag{47}$$

$$R \simeq a \gamma_{B,C}^{4/9} \frac{\alpha^{5/18} N_C^{\ 13/18}}{N_A^{1/6}} \tag{48}$$

$$H_C \simeq a \gamma_{B,C}^{4/9} \frac{N_C^{\ 13/18}}{\alpha^{13/18} N_A^{1/6}} \tag{49}$$

$$H_A \simeq a \gamma_{B,C}^{2/9} \frac{N_C^{1/9} N_A^{2/3}}{\alpha^{1/9}} \tag{50}$$

and the corresponding value of the free energy

$$\frac{F}{k_B T} \simeq \gamma_{B,C}^{5/9} \frac{N_C^{5/18} N_A^{1/6}}{\alpha^{5/18}} \tag{51}$$

Equations 49 and 50 indicate that when $N_A/N_A^* \ll \alpha^{-11/15}$ microsegregated cylindrical core is shielded by coronas *A* only partially, $H_A \leq H_C$, and free energy per molecule F (eq 51) is larger than in the equilibrium cylindrical micelle (eq 44). Therefore, the attractive interactions between unshielded portions of the core lead to collapse and precipitation of the aggregates from the solution (Figure 3b).

5. Diagram of States of the Solution

We summarize our finding in the diagram of states of the solution (Figure 4). The diagram is plotted in the reduced

variables, $N_A/N_A^* = N_A/(N_C^{11/15}\gamma_{B,C}^{4/15})$ and $\alpha = \gamma_{B,C}/\gamma$. It contains three regions: *St*, *Cyl*, and *G*.

In region *St* located at $N_A/N_A^* \geq 1$, the solution contains thermodynamically stable starlike spherical micelles. The equilibrium parameters of these micelles are given by eqs 18−21. When $\alpha \gg 1$, the core of a starlike micelle is almost spherical (*B*/*C* boundary passes through the center of the sphere) and the junctions are localized in a ribbon-shaped interfacial layer encircling *B*/*C* boundary. The free energy of the corona $F_{corona} \simeq p^{1/2} \ln(H_A/R)$ is governed by its peripheral part, and the aggregation number p exhibits a weak logarithmic dependence on the molecular weight of the soluble block N_A. When $\alpha \lesssim 1$, the core is dumbbell-shaped and the junctions detach from the core surface. When $\alpha < 1/2$, the junctions are localized in a belt of strings of thickness R_0. Conformation of such a micelle is analyzed in Appendix B. Because of transformation of the belt, the same power law dependences for the parameters of a starlike micelle hold at any value of α. Precipitation of such aggregates from the solution occurs when $N_A/N_A^* \simeq 1$.

In region *Cyl* an equilibrium micelle is of cylindrical shape. The core of such a micelle is laterally microsegregated into *B* and *C* domains of thickness $H_C = H_B$; the equilibrium parameters are given by eqs 41−44. The micelles are thermodynamically stable due to repulsion between coronas of component *A* ($H_A \gtrsim H_C$) and stay as wormlike cylinders in the solution. Resolution of the scaling model does not allow for thorough investigation of *St*−*Cyl* boundary, $N_A/N_A^* \simeq 1$. Here, intermediate soluble aggregates (supermicelles) may exist.

In sediment region *G*, the aggregates have microsegregated *B*/*C* core of locally cylindrical ($\alpha > 1$) or spherical ($\alpha < 1$) symmetry. Relatively small coronas of component *A* ($H_A < H_C$) are unable to shield the core of the aggregate, and the attractive interactions between the cores led to formation of a network of aggregates of various shapes. A detailed analysis of the properties of this phase is beyond the scope of this paper. When α is relatively large ($\alpha > \alpha^*$, see Discussion section), precipitation of the cylindrical micelles in sediment is accompanied by the cylinder-to-lamella transition (shown by dash-dotted line in Figure 4). Below this line, aggregates in sediment are expected to form lamellar mesophase.

6. Discussion

We present a scaling model of the spherical and the cylindrical micelles formed by 3-miktoarm *ABC* tercopolymer in a dilute solution. We focus mostly on the case of symmetric incompatible solvophobic blocks *B* and *C* ($N_C = N_B$). The solvent is poor for the arms *B* and *C* and is good for arms *A*. Our study demonstrates that two types of micelles can emerge in a dilute solution: starlike dumbbell micelles with corona thickness $H_A \gg R$ and cylindrical micelles with crew-cut corona, $H_A \ll R$.

When molecular weight of the soluble block *A* is large ($N_A \gg N_A^*$), the starlike micelles are thermodynamically stable. All the asymptotic scaling dependences for equilibrium parameters of starlike micelles formed by *ABC* 3-miktoarm stars or *AC* (*AB*) diblock copolymers are similar. The difference is on the level of numerical coefficients and details of the core structure. Segregation of components *B* and *C* in the core of *ABC* micelle leads to variation in the core shape as a function of ratio of the surface tension coefficients $\alpha = \gamma_{B,C}/\gamma$. When $\alpha \geq 1$, the shape of the core is determined by unfavorable interactions of monomers *B* and *C* with the solvent (the core of a starlike micelle is almost spherical). Junctions connecting all three blocks in 3-miktoarm copolymer are localized in ribbon-shaped belt encircling *B*/*C* boundary, and their contribution F_{belt} to micellar free energy per macromolecule $F \simeq F_{corona} \simeq F_{surface}$ is small. When $\alpha < 1$, the area of the *B*/*C* interface decreases, and the penalty for localization of junctions around *B*/*C* boundary increases. As a result, junctions start to detach from the belt, and the ribbon-to-strings transition takes place. The strings (strongly stretched segments of blocks *B* and *C* comprising junctions) link semicores *B* and *C* together. In this core configuration, the elastic free energy of core blocks F_{core} increases but still remains smaller than the micelle free energy $F \simeq F_{corona} \simeq F_{surface} \simeq F_{belt}$. As a result of core rearrangement, free energy F increases only by a numerical prefactor. (Note that logarithmic and other weak dependences are treated in our model as numerical coefficients.) Although starlike micelles become smaller with a decrease in $\alpha < 1$, the scaling exponents for aggregation number p, radius of the core R, thickness of the starlike corona H_A, and free energy per chain F remain unchanged. However, more weak (logarithmic) dependences may change as a function of α.

We consider also an asymmetric case, $\alpha_C \geq \alpha_B \geq 1$, when block *C* is more solvophobic than block *B* whereas the incompatibility of blocks *B* and *C* is relatively weak. In this case the core is almost spherical but consists of three segments: the central one is formed by blocks *C* and is capped and partially shielded from unfavorable contacts with solvent by two spherical segments formed by blocks *B*, Figure 1b (see Appendix A for details).

For relatively small molecular weight of soluble component *A* ($N_A < N_A^* \simeq \gamma_{B,C}^{4/15} N_C^{11/15}$), the behavior of 3-miktoarm *ABC* tercopolymers and *AC* (*AB*) diblock copolymers becomes dramatically different. Whereas diblock copolymer molecules associate in thermodynamically stable spherical micelles of crew-cut shape, the 3-miktoarm tercopolymer either aggregates in soluble crew-cut cylindrical micelles ($\alpha > 1$) or precipitates ($\alpha < 1$).

We emphasize that *AC* (*AB*) diblock copolymer associates in cylindrical micelles at lower molecular weight of the soluble block ($N_A = N_A^{sc} \simeq N_C^{2/3}\gamma_{B,C}^{1/3} < N_A^*$) than *ABC* copolymers. However, when both *ABC* and *AC* (*AB*) block copolymers form thermodynamically stable cylindrical micelles, their equilibrium parameters obey the same scaling laws. The difference is on the level of internal core structure: in *ABC* cylindrical micelle the core is laterally microsegregated, and coronas *A* stay at the verge of overlap, whereas in *AC* (*AB*) diblock copolymer cylindrical micelle the core is homogeneous, and the corona *A* is planar-like. Another difference concerns the region of stability of the cylindrical phase: when $\alpha \gtrsim 1$, *ABC* cylindrical micelles are stable in a wider range of molecular weight N_A, $\alpha^{-11/15} < N_A/N_A^* < 1$, whereas *AC* cylindrical micelles remain thermodynamically stable only in a narrow zone around $N_A^{sl} \simeq N_C^{2/3}\gamma_{B,C}^{1/3}$ (this zone is not specified in scaling terms; see ref 23 for details).

As already mentioned earlier, experimental observations on 3-miktoarm *ABC* micelles are rather sparse. Recent study[10] on 3-miktoarm polyethylethylene/poly(ethylene oxide)/polyperfluoropropylene star copolymer in dilute water solution indicated the presence of "spherically" shaped aggregates at relatively large molecular weight of water-soluble block *PEO* and of long wormlike micelles at smaller molecular weights of *PEO* block. Although χ parameters for these particular polymers are not equal, and *PEO* demonstrates rather sophisticated behavior in water,[21] the observed trend to form stable wormlike cylindrical micelles with a decrease in molecular weight of soluble block is consistent with our predictions. It is also in accord with the results of Monte Carlo simulation.[16]

Similarly to cylindrical micelles of *AC* (*AB*) diblock copolymer, *ABC* cylindrical micelles are expected to precipitate from the solution in the vicinity of cylinder(*C*)-to-lamella(*L*) transition. The physical origin of this transition is the same as for diblock copolymer micelles,[22,23] In both, a lamella and a cylindrical micelle dominant contributions to the free energy *F*

$\simeq F_{surface} + F_{corona}$ are equal. In a planar lamella the core block *C* is less constrained than in the core of a cylindrical micelle whereas coronal block *A* is more relaxed in the cylindrical corona. Balance of these corrections to free energy *F* allows for localization of *C*−*L* transition. For *AC* diblock copolymer *C*−*L* transition takes place when $N_A = N_A^{cl} \simeq N_A^{sc} \simeq N_C^{2/3}\gamma_{B,C}^{1/3} < N_A^*$.[23] Because of the same scaling for the parameters of *AC* and *ABC* cylindrical micelles (eqs 41−44), the *C*−*L* transition for *ABC* micelle is specified by the same power law dependence as for *AC* micelle, $N_A/N_A^* \simeq N_A^{cl}/N_A^* \simeq (\gamma_{B,C}/N_C)^{1/15}$. This boundary is parallel to α -axis and intersects the cylinder stability line $N_A/N_A^* \simeq \alpha^{-11/15}$ at

$$\alpha = \alpha^* \simeq (N_C/\gamma_{B,C})^{1/11} \tag{52}$$

When $\alpha > \alpha^*$, below this boundary formation of the lamellar (*L*) mesophase is expected in sediment. Although $N_C \gg 1$ and $\gamma_{B,C} < 1$, α^* can be reasonably small due to the small value of exponent $1/11 \approx 0.09$. Therefore, precipitation of cylindrical micelles from a dilute solution occurs upon intersection of either the cylinder stability line, $N_A/N_A^* \simeq \alpha^{-11/15}$ (when $1 < \alpha < \alpha^*$), or the *C*−*L* transition line, $N_A/N_A^* \simeq (\gamma_{B,C}/N_C)^{1/15}$ (when $\alpha > \alpha^*$). The width of the cylindrical corridor ΔN_A increases with an increase in α and reaches its maximal value, $\Delta N_A \simeq N_A^*[1 - (\gamma_{B,C}/N_C)^{1/15}]$, when $\alpha \gtrsim \alpha^* \simeq (N_C/\gamma_{B,C})^{1/11}$. When $\alpha \lesssim 1$, the width of cylindrical phase is not specified in scaling terms.

In conclusion, we predict that in a selective solvent 3-miktoarm *ABC* tercopolymer with incompatible solvophobic blocks associates in starlike spherical or crew-cut cylindrical micelles. Segregation of *B* and *C* components in the core of *ABC* micelle governs the equilibrium configuration of the core which is sensitive to the ratio of surface tensions γ and $\gamma_{B,C}$ at polymer−polymer and polymer−solvent interfaces. However, the asymptotic power law dependences for equilibrium parameters of such micelles are the same as for *AC* diblock copolymer micelles under similar conditions. The stability region of *ABC* cylindrical micelle is delineated in scaling terms and increases with an increase in ratio $\alpha = \gamma_{B,C}/\gamma > 1$.

Acknowledgment. This work has been partially supported by the Russian Foundation for Basic Research, grant 05-03-33126, and by the joint program of Dutch National Science Foundation (NWO) and Russian Foundation for Basic Research "Polymers in nanomedicine: design, synthesis and study of interpolymer and polymer-virus complexes in search for novel pharmaceutical strategies", grant 06-04-89402.

Appendix A. Asymmetric Interaction of the Core-Forming Blocks with the Solvent

For the asymmetrical case we focus only on the limit of strong solvophobicity of the both core forming blocks, i.e., $\alpha_C \geq \alpha_B \geq 1$. In this case the core as a whole retains almost spherical shape but contains two internal *B*/*C* interfaces between the central (*C*) region formed by more solvophobic blocks *C* and the "caps" formed by less solvophobic blocks *B* (Figure 1b). The radius *R* of the core is given by the mass conservation condition

$$R = \left[\frac{3p}{4\pi}(N_B + N_C)\right]^{1/3}$$

In this case, there are two *B*/*C* interfaces with radii $R_b = R(1 - \zeta^2)^{1/2}$, where *R* is the radius of the core and $\zeta \approx 0.35$ is the root of the equation $\zeta^3 - 3\zeta + 1 = 0$, which follows from equality of total volumes $V_B = V_C$ occupied by *B* and *C* blocks within the core. The total area of the *B*/*C* interface is $2\pi R_b^2 = 2\pi R^2(1 - \zeta^2)$. The areas of interface between the condensed block *C* and the solvent and between the condensed block *B* and the solvent are $4\pi R^2\zeta$ and $4\pi R^2(1 - \zeta)$, respectively. The corresponding interfacial free energy is given by

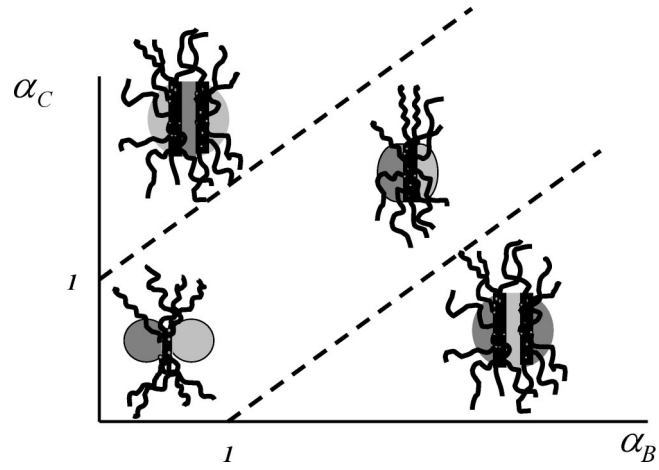

Figure 5. Diagram of states of the solution of 3-miktoarm *ABC* tercopolymer as a function of relative solvophobicity of core-forming blocks *B* and *C*.

$$\frac{F_{surface}}{k_B T} = 2\pi R^2[\gamma(1 - \zeta^2) + 2\gamma_B(1 - \zeta) + 2\gamma_C\zeta] \tag{53}$$

where the first term accounts for the contribution of the *B*/*C* interface whereas the second and the third terms are the respective surface free energies of condensed domains *B* and *C*.

This free energy should be compared to the corresponding free energy of a spherical core comprising one hemispherical domain *B* and one hemispherical domain *C*

$$\frac{F_{surface}}{k_B T} = \pi R^2[\gamma + 2(\gamma_B + \gamma_C)] \tag{54}$$

One can easily see that the interfacial free energy of the core comprising one *C* and two *B* subdomains ("hamburger-like" structure) is lower than that of the core consisting of *B* and *C* hemispheres provided

$$\gamma_C \geq \gamma_B + \gamma\frac{1 - 2\zeta^2}{2(1 - 2\zeta)} \approx \gamma_B + \gamma \tag{55}$$

Within the accuracy of the scaling approximation, the coronal contribution to the micelle free energy is the same for both structures of the core to be compared. Therefore, the value of γ_C given by eq 55 can be considered as an upper estimate for the condition of split of the hemispherical core *B* into two segments capping the central domain *C*. The schematic phase diagram for two possible structures of micelles with quasi-spherical core, $\alpha_B, \alpha_C \geq 1$, is presented in Figure 5. The diagram contains the region corresponding to micelles with a core consisting of two hemispheres (at weak asymmetry of polymer–solvent interactions) and two regions corresponding to micelles with a core comprising three subdomains (hamburger-like structure with central domain *C* and capping domains *B* at $\gamma_C \geq \gamma_B$ and inverse structure with central domain *B* and capping domains *C* at $\gamma_B \geq \gamma_C$).

Clearly, within applied here scaling approximation split of the core domain *B* into two subdomains does not affect power law dependences for the properties of spherical and particularly cylindrical micelles as well as the boundaries between different regimes in the phase diagram.

Appendix B. Structure of Starlike Micelle in the Strong Segregation Limit $\alpha \ll 1$

In this Appendix we demonstrate that when $\chi \gg 1$ (or, equivalently, $\alpha \ll 1$), the scaling dependences for equilibrium

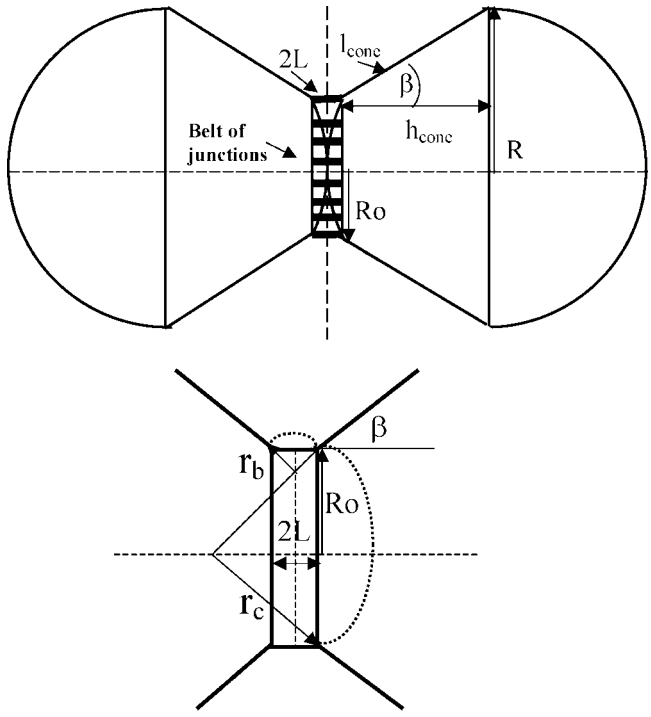

Figure 6. Schematic of micellar core configuration assumed in Appendix B in calculation of the equilibrium characteristics of starlike micelles in the limit of strong incompatibility between solvophobic blocks *B* and *C*.

characteristics of a starlike micelle retain the same exponents as in the case of $\alpha \geq 1$.

We assume that when $\alpha \ll 1$, the junction belt transforms into a belt of strings comprising junction points. Each string comprises strongly stretched segments of monomers *B* and *C* (shown by thick black lines in Figure 6), and the junction point can be located anywhere inside the string. This situation is reminiscent of pulling out the chain end from a collapsed polymer globule.[24] We assume that both cores *B* and *C* are partly spherical and partly conical to decrease confinement of polymer segments *A* between the cores (see schematic of micelle cross section in Figure 6). As before, free energy *F* per chain yields

$$F = F_{\text{surface}} + F_{\text{belt}} + F_{\text{corona}} + F_{\text{core}} \tag{56}$$

Surface Free Energy. For specific configuration of the micellar core depicted in Figure 6 the surface free energy per chain is given by

$$\frac{F_{\text{surface}}}{k_{\text{B}}T} = \frac{2\gamma_{B,C}}{p}(4\pi R^2 - 2\pi R h_{\text{cone}} + \pi(R_0 + R)l_{\text{cone}})$$

$$= \frac{2\pi\gamma_{B,C}R^2}{p}(4 - 2\sqrt{1-x^2} + (1+x)\sqrt{2(1-x)}) \tag{57}$$

where $h_{\text{cone}} = (R^2 - R_0^2)^{1/2} = R(1-x^2)^{1/2}$, $l_{\text{cone}} = [h_{\text{cone}}^2 + (R - R_0)^2]^{1/2} = R[2(1-x)]^{1/2}$, and $x = R_0/R < 1$. Note that $\cos\beta = [(1+x)/2]^{1/2}$ and $\sin\beta = [(1-x)/2]^{1/2}$. The volume of core *C* (or *B*) yields

$$V_C = \frac{4\pi}{3}R^3 - \frac{\pi}{3}h_{\text{cone}}(2R^2 + R_0^2) + \frac{\pi}{3}h_{\text{cone}}(R^2 + RR_0 + R_0^2)$$

$$= \frac{\pi}{3}R^3(4 - (1-x)\sqrt{1-x^2}) \tag{58}$$

By equating $V_C = a^3 p N_C$, we find the relationship between aggregation number *p* and core radius *R*

$$R/a = \left(\frac{3pNc}{\pi}\right)^{1/3} \frac{1}{\left(4 - (1-x)\sqrt{1-x^2}\right)^{1/3}} \tag{59}$$

By substituting eq 59 in eq 57, we find

$$\frac{F_{\text{surface}}}{k_{\text{B}}T} \simeq \frac{\gamma_{B,C}N_C^{2/3}}{p^{1/3}} \frac{(4 - 2\sqrt{1-x^2} + (1+x)\sqrt{2(1-x)})}{\left(4 - (1-x)\sqrt{1-x^2}\right)^{2/3}} \tag{60}$$

Belt Free Energy. We envision the belt of strings as a regular array of rods with rod thickness $\simeq a$ and inter-rod distance *d*. The strings are connecting two spheres of radius *R*, and the total number of strings is *p*. The layer of rods at distance $x_k = kd$ from the core axis comprises $p_k \simeq 2\pi x_k/d \simeq k$ rods. Therefore, the total number of rods $p \simeq \sum_k p_k \simeq m^2$ where $m = R_0/d$ is the total number of layers and $R_0 < R$ is the outer radius of the belt. Length l_k of the string in layer *k*

$$l_k = R - \sqrt{R^2 - x_k^2} \simeq \frac{x_k^2}{R} \tag{61}$$

The average length of rods in the belt is

$$L = \frac{\sum_k l_k p_k}{p} \simeq \frac{\sum_k d_k^2 k^3}{Rp} \simeq \frac{d^2 m^2}{R} \simeq \frac{R_0^2}{R} \tag{62}$$

whereas the average thickness of the belt is

$$\frac{\sum_k x_k p_k}{p} \simeq dm = R_0 \tag{63}$$

Each chain segment *A* passing between the rods is found in an effective tube of width *d* and produces the blobs of size *d*. To decrease the free energy losses (number of blobs times $k_{\text{B}}T$), a segment *A* starting in layer *k* produces minimal number of such blobs, $m - k$. Note that when contacts between the chain and the tube are highly unfavorable ($\chi \gg 1$), effective size of the tube diminishes as $d - a$. (When $d \gg a$, the effective size of the tube is still $\simeq d$.) The average number of the blobs per chain is

$$\frac{\sum_k (m-k)p_k}{p} \simeq m^3/p \simeq p^{1/2} \tag{64}$$

whereas volume fraction φ_{blob} of the blobs at the outer boundary of the belt (layer *m*) is

$$\varphi_{\text{blob}} \simeq \frac{x_m l_m}{d^2 p} \simeq \frac{R_0^3}{Rd^2m^2} \simeq \frac{R_0}{R} < 1 \tag{65}$$

and therefore the blobs do not overlap inside the belt. Area per chain s_0 at the outer boundary of the belt is

$$s_0 \simeq \frac{LR_0}{p} \simeq \frac{R_0^3}{Rp} \tag{66}$$

whereas interstring distance *d* is related to area s_0 as

$$d \simeq \frac{R_0}{p^{1/2}} \simeq \sqrt{s_0 \frac{R}{R_0}} > \sqrt{s_0} \tag{67}$$

The belt free energy per chain yields

$$\frac{F_{\text{belt}}}{k_{\text{B}}T} \simeq p^{1/2} + L(1 + \gamma_{B,C}) \simeq p^{1/2} + \frac{R_0^2}{R} \tag{68}$$

where the first (independent of R_0) term is due to the interactions between segments *A* and the strings whereas the second term is the free energy of elastic stretching of the strings ($\gamma_{B,C} \lesssim 1$). By introducing $x = R_0/R$ and substituting *R* from eq 59, we finally obtain

$$\frac{F_{\text{belt}}}{k_{\text{B}}T} \simeq p^{1/2} + \frac{x^2(pN_C)^{1/3}}{\left(4-(1-x)\sqrt{1-x^2}\right)^{1/3}} \tag{69}$$

When $x \ll 1$ (strong deformation of the core)

$$\frac{F_{\text{belt}}}{k_{\text{B}}T} \simeq p^{1/2} + x^2(pN_C)^{1/3} \tag{70}$$

Coronal Free Energy. Coronal free energy F_{corona} comprises contribution F_{A0} due to segments A confined in the gap between cores B and C and the contribution due to external (starlike) part of the corona (eq 11),

$$\frac{F_{\text{corona}}}{k_{\text{B}}T} = \frac{F_{A0}}{k_{\text{B}}T} + p^{1/2}\ln\left(\frac{H_A}{R}\right) \tag{71}$$

where $F_{A0}/k_{\text{B}}T$ is evaluated as total number of the blobs filling the space between cores B and C. To simplify this calculation, we approximate the cylindrical surface of junction belt by a barrel type surface with radius of curvature

$$r_b = \frac{L}{\cos(\beta)} < R_0 \tag{72}$$

Then area $\Sigma(r)$ available for chains A at distance r from the axis is

$$\Sigma(r) = 4\pi r\int_{\beta}^{\pi/2} \mathrm{d}\varphi\ [r\sin(\varphi) + R_0 - r_b\sin(\beta)] \approx 4\pi r\left[r\cos(\beta) + R_0\left(\frac{\pi}{2}-\beta\right)\right] \tag{73}$$

where $r_b\sin(\beta)$ is neglected with respect to R_0. The total number of blobs with size $\xi(r) \simeq [\Sigma(r)/p]^{1/2}$ in the gap between cores B and C is evaluated as

$$\frac{F_{A0}}{k_{\text{B}}T} \simeq \int_{r_b}^{r_b+[(R-R_0)/\cos(\beta)]} \frac{\mathrm{d}r}{\xi(r)} \simeq \int_{r_b}^{r_b+[(R-R_0)/\cos(\beta)]} \frac{\mathrm{d}r}{\sqrt{\Sigma(r)/p}} \simeq \frac{p^{1/2}}{\sqrt{\cos(\beta)}}\int_{r_b}^{r_b+[(R-R_0)/\cos(\beta)]} \frac{\mathrm{d}r}{\sqrt{r(r+b)}} \tag{74}$$

where $b = R_0(\pi/2 - \beta)/\cos(\beta)$ After performing integration in eq 74

$$\int \frac{\mathrm{d}r}{\sqrt{r(r+b)}} = 2\ln(\sqrt{r+b} + \sqrt{r})$$

we find that when $x = R_0/R \ll 1$

$$\frac{F_{A0}}{k_{\text{B}}T} \simeq \frac{p^{1/2}}{\sqrt{\cos(\beta)}}\ln\left(\frac{R}{R_0}\right) \simeq \frac{p^{1/2}}{(1+x)^{1/4}}\ln\left(\frac{1}{x}\right) \simeq p^{1/2}\ln\left(\frac{1}{x}\right) \tag{75}$$

The total coronal free energy per macromolecule is therefore given by

$$\frac{F_{\text{corona}}}{k_{\text{B}}T} \simeq p^{1/2}\left[\ln\left(\frac{H_A}{R}\right) + \ln\left(\frac{1}{x}\right)\right] \tag{76}$$

Core Free Energy. In the limit $\chi \gg 1$, blocks B (C) are uniformly tethered to the surface of spherical core C (B) with radius of cross section R_0. To simplify calculation, we substitute the concave spherical surface of core C inside the belt by a convex spherical surface with radius of curvature

$$r_c = R_0/\sin(\beta) \tag{77}$$

Locally, portions of chains C (B) inside each core constitute dense spherical brushes. The area $\Sigma(r)$ available for chains C (B) at distance r from the center of curvature is given by

$$\Sigma(r) = 2\pi\int_0^{\beta} r^2\sin(\varphi)\,\mathrm{d}\varphi = 2\pi r^2[1-\cos(\beta)]$$

In such a brush local stretching of a chain $\mathrm{d}r/\mathrm{d}n$ at distance r is

$$\frac{\mathrm{d}r}{\mathrm{d}n} \simeq \frac{pa^3}{\Sigma(r)} \simeq \frac{pa^3}{r^2[1-\cos(\beta)]} \tag{78}$$

and the elastic stretching in the conical part of the core is given by

$$\frac{F_{\text{core}}}{k_{\text{B}}T} \simeq \frac{3}{2a^2}\int_{r_c}^{r_c+[(R-R_0)/\sin(\beta)]} \frac{\mathrm{d}r}{\mathrm{d}n}\,\mathrm{d}r \simeq \frac{pa}{1-\cos(\beta)}\int_{R_0/\sin(\beta)}^{R/\sin(\beta)} \frac{\mathrm{d}r}{r^2} \simeq \frac{\sin(\beta)}{1-\cos(\beta)}\frac{p}{R_0} \simeq \frac{p}{R_0} \tag{79}$$

In the second half of the core the free energy of elastic stretching is $\simeq R^2/a^2N_C \simeq p/R$. By introducing $x = R_0/R \ll 1$, we finally find

$$\frac{F_{\text{core}}}{k_{\text{B}}T} \simeq \frac{p}{R}\left(\frac{1}{x}\right) \simeq \frac{R^2}{a^2N_C}\left(\frac{1}{x}\right) \tag{80}$$

Starlike Micelle. When $x \ll 1$, the leading terms in free energy F per chain in a starlike micelle are

$$\frac{F}{k_{\text{B}}T} \approx \frac{F_{\text{corona}} + F_{\text{surface}} + F_{\text{belt}}}{k_{\text{B}}T} \simeq p^{1/2}\left(K + \ln\frac{1}{x}\right) + \frac{\gamma_{B,C}N_C^{2/3}}{p^{1/3}}[1 - 0(x)] + x^2(pN_C)^{1/3} \tag{81}$$

Minimization of free energy $F = F(p, x)$ with respect to x gives (with accuracy of numerical prefactors)

$$-\frac{p^{1/2}}{x} - \frac{\gamma_{B,C}N_C^{2/3}}{p^{1/3}} + x(pN_C)^{1/3} = 0 \tag{82}$$

By balancing the first and the third terms in eq 82, we obtain

$$x = x_0 \simeq \frac{p^{1/12}}{N_C^{1/6}} \tag{83}$$

The second term in eq 82 can be ignored when $p \gg N_C^{2/3}$. The free energy per chain is now given by

$$\frac{F}{k_{\text{B}}T} \simeq p^{1/2}\left(K + \ln\frac{1}{x_0}\right) + \frac{\gamma_{B,C}N_C^{2/3}}{p^{1/3}} \tag{84}$$

where the numerical coefficients are omitted.

Second minimization of free energy F with respect to p gives

$$p \simeq \gamma_{B,C}^{6/5}N_C^{4/5}\left(K + \ln\frac{1}{x_0}\right)^{-6/5} \tag{85}$$

and the second term in eq 82 can be indeed neglected. With the accuracy of logarithmic corrections core radius R is given by

$$R/a \simeq \gamma_{B,C}^{2/5}N_C^{3/5} \tag{86}$$

and the equilibrium free energy per chain is

$$\frac{F}{k_{\text{B}}T} \simeq \gamma_{B,C}^{3/5}N_C^{2/5} \tag{87}$$

We therefore recover the same scaling exponents for the micelle parameters as in the case of $\alpha > 1$. The difference is on the level of weak logarithmic dependences.

The thickness of junction belt is

$$R_0 = Rx_0 \simeq R\frac{p^{1/12}}{N_C^{1/6}} \simeq \sqrt{\gamma_{B,C}N_C} \quad (88)$$

whereas average length of the string is

$$L \simeq R_0^2/R \simeq a\gamma_{B,C}^{3/5}N_C^{2/5} \quad (89)$$

We emphasize that the considered configuration of the core is not necessarily the optimal one (corresponding to the global minimum of the micelle free energy). However, even in this configuration the scaling exponents remain unchanged.

We also note that below boundary $N_A/N_A^* \simeq 1$ such micelles are expected to precipitate. Similarly to the case of $\alpha \gg 1$ rearrangement into stable cylindrical micelle requires an increase in R and a decrease in p. This would lead to pulling of coronal blocks A in the gap between cores B and C and exposure of core surfaces.

Appendix C. Localization of Junctions in a Starlike Micelle

We consider two cases: beltlike (a) and uniform (b) distributions of the junction monomers at the surface of a spherical core with radius R. The core contains p blocks B and C; the area of the core/corona interface is $s \simeq R^2/p$ per block. The insoluble components B and C separate to avoid the free energy penalty $\simeq k_BT\chi N_C$ per block (B or C) due to B/C contacts. They can either form two hemispheres with single B/C boundary of area $\simeq R^2$ or undergo microsegregation into domains inside the core with multiple B/C boundaries. In both cases, the surface free energy at the core/corona interface stays the same whereas the surface free energy due to multiple B/C boundaries increases by $\Delta F_{surface}$ per macromolecule.

Because of the composition symmetry ($N_B = N_C$), microsegregated domains B and C can be approximated by the cones with area of the base $\Sigma \simeq fs$ where f is the number of B and C blocks within a single domain (B or C). Formation of such domains under the constraint of uniform spreading of junctions at the core surface requires passage of segments of blocks B (C) with average number of monomers n through domain C (B) at distance $\simeq \Sigma^{1/2} \simeq (fs)^{1/2}$. By minimizing the elastic stretching of the segments, $\delta F_{elastic}/k_BT \simeq \Sigma/na$, with the interaction free energy penalty for passage, $\delta F_{interaction}/k_BT \simeq \chi n$, we find number of monomers $n \simeq (\Sigma/a^2\chi)^{1/2}$ and the corresponding free energy of the segment

$$\delta F_{segment}/k_BT = \delta F_{elastic}/k_BT + \delta F_{interaction}/k_BT \simeq \sqrt{\chi fs} \quad (90)$$

Surface free energy per macromolecule associated with conical B/C boundaries is

$$\delta F_{surface}/k_BT \simeq \frac{\gamma R\sqrt{\Sigma}}{f} \simeq \frac{R}{a}\sqrt{\frac{\chi s}{f}} \quad (91)$$

By balancing $\delta F_{segment} \simeq \delta F_{surface}$, we find the equilibrium value of $f \simeq R/a$, and the decrease in the surface free energy due to gathering junctions in the belt

$$\Delta F_{surface}/k_BT \simeq \gamma\left(\frac{R^2}{p} - \sqrt{Rsa}\right) \simeq \gamma(s - \sqrt{Rsa}) \simeq -\gamma\sqrt{Rsa} \quad (92)$$

provided that $Ra \gg s$.

The equilibrium properties of a starlike micelle are determined by the balance of the overall surface free energy $F_{surface}$ and the coronal free energy F_{corona}. At distances $r \gg R$ from the core, the blob structure of the corona is the same in both cases (a) and (b). At distances $r \ll R$ (where the corona is quasiplanar), gathering of junctions in a belt (that is, transformation of planar-like brush with thickness R and the free energy $R/\sqrt{s} \simeq p^{1/2}$ into a cylindrical brush with linear grafting density $\rho \simeq p/R$ and thickness $\simeq R$ would lead to an increase in the coronal free energy by

$$\Delta F_{corona}/k_BT \simeq (R\rho)^{1/2} - p^{1/2} \simeq p^{1/2}$$

per macromolecule (see eqs 12 and 13).

In a starlike micelle with symmetric insoluble blocks ($N_B = N_C$), scaling dependence for core radius $R \sim aN_C^{3/5}$ (eq 22) ensures the inequality $Ra \gg s \sim a^2N_C^{2/5}$. As a result, the decrease in the free energy of B/C interface due to localization of junctions in the belt, $\Delta F_{surface}/k_BT \simeq (Rsa)^{1/2} \simeq -N_C^{1/2}$, is asymptotically larger than the increase in coronal free energy due to chain crowding, $\Delta F_{corona}/k_BT \simeq p^{1/2} \simeq N_C^{2/5}$, when $N_C \gg 1$. Therefore, a spherical micelle with the junction belt encircling single B/C boundary is thermodynamically more stable than a micelle with microsegregated core with multiple B/C boundaries and junctions uniformly distributed over the core surface.

References and Notes

(1) Fleer, G. J.; Cohen Stuart, M. A.; Scheutjens, J. M. H. M.; Cosgrove, T.; Vincent, B. *Polymers at Interfaces*; Chapman & Hall: London, 1993.
(2) Hamley, I. W. *The Physics of Block Copolymers*; Oxford University Press: New York, 1998.
(3) Riess, G. *Prog. Polym. Sci.* **2003**, *28*, 1107.
(4) Kabanov, A. V.; Batrakova, E. V.; Alakhov, V. Y. *J. Controlled Release* **2002**, *82*, 189.
(5) Fustin, C.-A.; Abetz, V.; Gohy, J.-F. *Eur. Phys. J. E* **2005**, *16*, 291.
(6) Fujimoto, T.; Zhang, H.; Kazama, Y.; Isono, Y.; Hasegawa, H.; Hashimoto, T. *Polymer* **1992**, *33*, 2008.
(7) Sioula, S.; Hadjichristidis, N.; Tomas, E. L. *Macromolecules* **1998**, *31*, 8429.
(8) Sioula, S.; Tselicas, N.; Hadjichristidis, N. *Macromolecules* **1997**, *30*, 1518.
(9) Hadjichristidis, N.; Pispas, S.; Patrikalis, M.; Iatrou, H.; Viahos, C. *Adv. Polym. Sci.* **1999**, *142*, 71.
(10) Li, Z.; Kasselman, E.; Talmon, Y.; Hillmayer, M. A.; Lodge, T. P. *Science* **2004**, *06*, 98.
(11) Takano, A.; Wada, S.; Sato, S.; Araki, T.; Hirahara, K.; Kazama, T.; Kawahara, S.; Isono, Y.; Ohno, A.; Tanaka, N.; Matsushita, Y. *Macromolecules* **2004**, *37*, 9941.
(12) He, X. H.; Huang, L.; Liong, H. J.; et al. *J. Chem. Phys.* **2002**, *116*, 10508.
(13) He, X. H.; Huang, L.; Liong, H. J.; Pan, C. *J. Chem. Phys.* **2003**, *118*, 9861.
(14) Birshtein, T. M.; Polotsky, A.; Abetz, V. *Macromol. Theor. Simul.* **2004**, *13*, 512.
(15) Gemma, T.; Hatono, A.; Dotera, T. *Macromolecules* **2002**, *35*, 3225.
(16) Zhu, Y.; Li, R. K. Y.; Jiang, W. *Chem. Phys.* **2006**, *327*, 137.
(17) Daoud, M.; Cotton, J.-P. *J. Phys. (Paris)* **1982**, *43*, 531.
(18) Birshtein, T. M.; Zhulina, E. B. *Polymer* **1984**, *25*, 1453.
(19) (a) Zhulina; Ye. B; Birshtein, T. M. *Polym. Sci. USSR* **1985**, *27*, 570. (b) Birshtein, T. M.; Zhulina, E. B. *Polymer* **1989**, *30*, 170.
(20) Semenov, A. M. *Sov. Phys. JETP* **1985**, *61*, 733.
(21) Dormidontova, E. *Macromolecules* **2002**, *35*, 987.
(22) Borisov, O. V.; Zhulina, E. B. *Macromolecules* **2003**, *36*, 10029.
(23) Zhulina, E. B.; Adam, M.; Sheiko, S.; LaRue, I.; Rubinstein, M. *Macromolecules* **2005**, *38*, 5330.
(24) Halperin, A.; Zhulina, E. B. *Europhys. Lett.* **1991**, *15*, 417.

MA702369G